DAMAGE ASSESSMENT OF H-SECTION STEEL COLUMNS UNDER VEHICLE EXPLOSIONS

SIQI CHEN & WEIFANG XIAO
College of Civil Engineering, Tongji University, China

ABSTRACT
To evaluate the damage levels of H-section steel columns in steel frame structures under vehicle explosions, this study adopts a blast scenario similar to the Oklahoma City bombing (passenger/cargo van with a TNT equivalent mass of 1,814 kg). Five standoff distances (R = 6, 7, 8, 9 and 10 m) and three angles of incidence (α = 0°, 45° and 90°) are considered to analyse the damage modes and residual load-bearing capacity of a full-scale steel column. Numerical simulations are conducted to capture the dynamic response and failure mechanisms of the column under blast loading. The results reveal that the columns may exhibit various failure modes, including tearing at flange–web connections, shear fracture at the base, global bending and torsion, and local buckling, depending on the standoff distance and angle of incidence. The study also quantifies the residual load-bearing capacity corresponding to each damage mode, providing a basis for evaluating the post-blast performance of steel columns. These findings offer valuable insights for the design and retrofitting of steel frame structures to enhance their resilience against vehicle explosions.
Keywords: steel column, damage mode, damage assessment, vehicle explosion.

1 INTRODUCTION

In steel frame structures, columns are one of the primary load-bearing components. The loss of load-bearing capacity and stiffness softening of steel columns under blast loading can lead to the collapse of the entire structure. For instance, the 1995 Oklahoma City bombing of the Murrah Federal Building, which resulted in 168 fatalities, demonstrated the catastrophic consequences of vehicle explosions. This incident has spurred increasing research interest in the blast resistance of structures. Inspired by this event, Magallanes et al. [1] replaced the concrete columns of the Murrah Building with steel columns and conducted full-scale blast tests to study the response of steel columns under similar explosion conditions. Their results showed no significant local fractures, highlighting the excellent ductility of structural steel. Similarly, Morrill et al. [2] conducted full-scale blast tests on steel columns subjected to vehicle-borne and satchel charge explosions, observing localized fractures in the columns. Due to the high cost and logistical challenges of full-scale tests, many researchers have turned to scaled experiments to study the blast performance of steel columns. For example, Grisaro et al. [3]–[5] performed close-in blast tests and numerical simulation of steel wide-sections to examine their dynamic response under shock waves along the strong and weak axes. They analysed deformation modes, including global bending and local deformation under certain conditions. Remennikov and Uy [6] investigated the behaviour of square hollow steel tubular columns under contact and near-field blast scenarios, comparing the failure mechanisms of hollow and concrete-filled tubes. Additionally, Gangolu and Grisaro [7] studied the influence of axial load ratio (ALR) on the residual load-bearing capacity of steel columns, focusing on the P-δ effect.

In this study, a numerical model is developed using LS-DYNA to investigate the effects of standoff distance and angle of incidence on the damage modes and residual load-bearing capacity of a full-scale steel column under an explosion with the TNT equivalent mass of 1,814 kg, representing a passenger/cargo van explosion.

WIT Transactions on The Built Environment, Vol 215, © 2025 WIT Press
www.witpress.com, ISSN 1743-3509 (on-line)
doi:10.2495/SUSI250091

2 NUMERICAL MODELS AND VALIDATION

A three-dimensional finite element model, incorporating high explosive, air, and steel column, was developed using LS-DYNA. To validate the model and methodology, a series of experiments conducted by Nassr et al. [8], [9] and Zhao et al. [10] were simulated.

2.1 Establishment of numerical model

The S-ALE (Structured Arbitrary Lagrangian–Eulerian) method is employed in this study, where the air domain is not explicitly modelled but defined using *ALE_STRUCTURED_MESH to specify the air mesh and corresponding coordinates. The detonation location and geometry of the explosive are defined using *INITIAL_DETONATION and *ALE_STRUCTURED_MESH_VOLUME_FILLING. The fluid–structure interaction (FSI) process is established through the keyword *ALE_STRUCTURED_FSI. The air boundaries are set using *BOUNDARY_SALE_MESH_FACE. In this study, the steel column is positioned vertically on the ground, and ground effects are considered in the analysis.

TNT is selected as the high explosive, with its material properties and equation of state defined using *MAT_HIGH_EXPLOSIVE_BURN and *EOS_JWL. Air is modelled as an ideal gas using *MAT_NULL and *EOS_LINEAR_POLYNOMIAL. The steel column incorporates the Cowper–Symonds material model to account for strain rate effects, with its material properties defined by *MAT_PLASTIC_KINEMATIC, a yield strength of 459 MPa, and parameters $C = 6{,}844\ s^{-1}$ and $P = 3.91$. Given the wide range of standoff distances studied (6–10 m), a fixed air mesh size is unsuitable. Therefore, the mesh convergence is determined by comparing the reflected impulse for air mesh sizes of $R/50$, $R/100$, $R/150$, and $R/200$ at $R = 7.0$ m and $\alpha = 0°$, as shown in Fig. 1. Since the results for $R/150$ and $R/200$ differ by only 3.9%, $R/150$ is selected as the air mesh size. For the steel column mesh, a size of 2 cm is chosen based on comparisons with experimental responses.

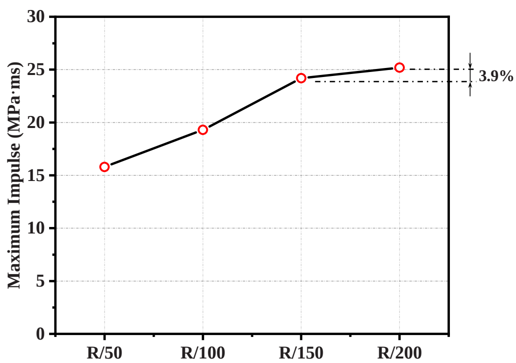

Figure 1: Mesh convergence for maximum impulses versus mesh sizes under scenario $R = 7.0$ m, $\alpha = 0°$.

This study employs a four-stage simulation method, as illustrated in Fig. 2. The four stages include:

- Step I: preloading of the axial force on the steel columns;
- Step II: shock wave propagation and its interaction with the steel columns;

- Step III: free oscillation of the steel columns;
- Step IV: axial loading phase for the residual capacity of steel columns after the blast.

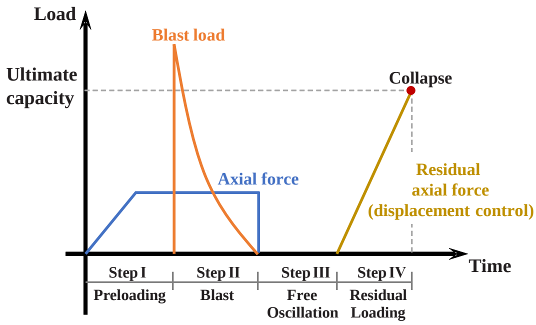

Figure 2: Numerical algorithm.

2.2 Validation of numerical model

To the best of the authors' knowledge, no tests have been conducted on steel columns that comprise all four stages mentioned above. Therefore, two separate experiments were used to simulate these stages individually.

The first experiment involves the blast tests on H-section steel columns conducted by Nassr et al. [8], [9]. The experimental setup and the quarter-symmetric finite element model are shown in Fig. 3. In the validated scenario, 100 kg of ANFO explosive was placed 10.3 m from the structure. Since the scaled distance exceeds 1.0 m/kg$^{1/3}$, the shape effect of the explosive can be neglected, and it is modelled as a sphere. The geometric dimensions of the steel column are $b \times h \times h_w \times h_f = 102 \times 160 \times 7 \times 10$ mm, where h and b are the sectional height and width, and h_f and h_w are the thicknesses of the flange and web. The column is supported by a hinge at the top and a roller support at the bottom. Plywood panels in between two neighboured column prevents shockwave diffraction and is modelled as a flexible body with a failure strain of 0.25 to control material erosion. The displacement–time history curve at the midpoint of column 2C1 and the simulated residual deformation of the three columns after the blast are shown in Fig. 4 and Fig. 5, exhibiting a good agreement with the experimental data.

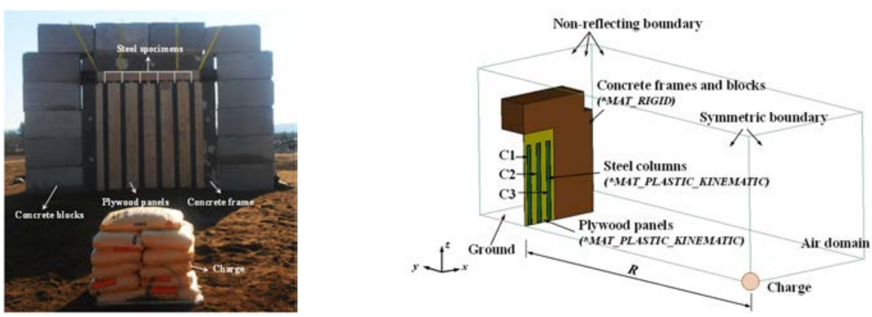

(a) (b)

Figure 3: Nassr's test: (a) Blast test setup [8], [9]; and (b) corresponding FE model.

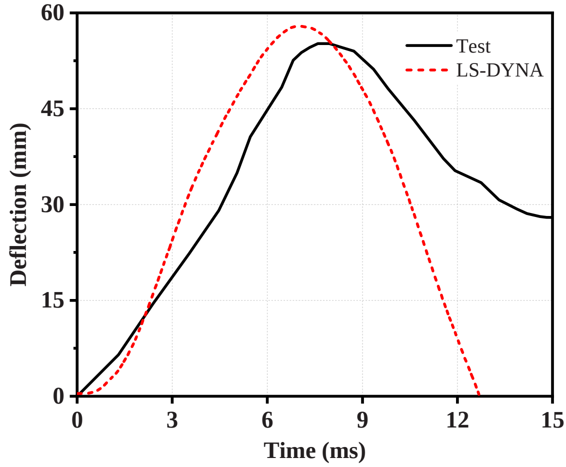

Figure 4: Deflection–time history of column 2C1.

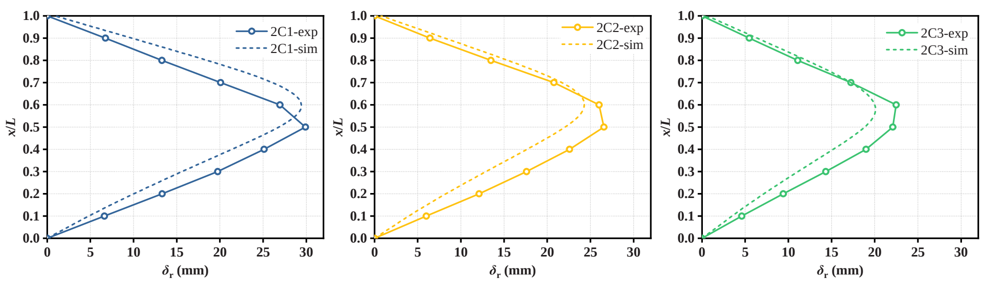

(a) (b) (c)

Figure 5: Residual deflection profile δ_r of 2C1, 2C2 and 2C3. (Note: x is the elevation of the gauge porin from the ground; L is the height of the columns.)

The second experiment involves the load-bearing capacity tests on steel columns conducted by Zhao et al. [10]. The experimental setup is shown in Fig. 6. Displacement-controlled loading was applied at rates ranging from 0.1 to 10 cm/s, and the load-lateral displacement curves and load-bearing capacities at different loading rates are presented in Fig. 7. At a loading rate of 1 cm/s, the simulated load-bearing capacity is 605.2 kN, which shows a relative error of 4.83% compared to the experimentally measured capacity of 577.3 kN. Therefore, a loading rate of 1 cm/s is selected for evaluating the post-blast residual load-bearing capacity.

3 PARAMETRIC STUDY

3.1 Geometry of the designed steel columns and scenarios

This study focuses on H-section steel columns with dimensions HW 350 × 350 ($b \times h \times h_w \times h_f$ = 350 × 350 × 12 × 19 mm), which were used as ground-floor columns in an actual steel

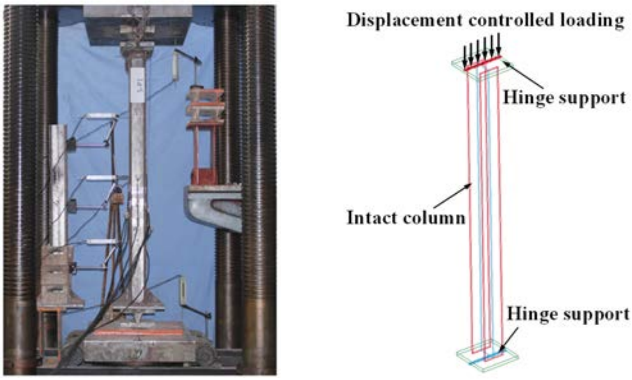

(a) (b)

Figure 6: Test of residual bearing capacity of the steel column. (a) Test setup; and (b) Numerical model.

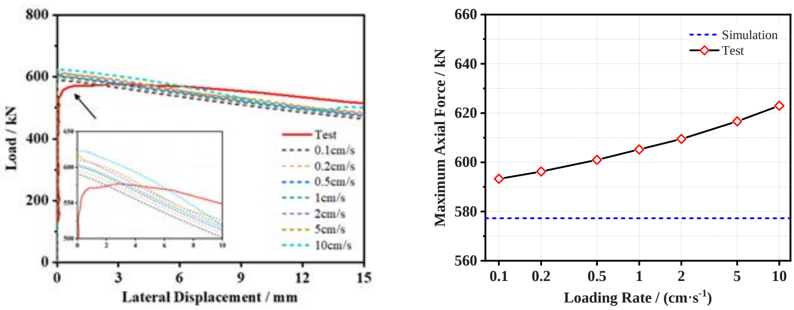

(a) (b)

Figure 7: Numerical results. (a) Axial load-lateral displacement curves; and (b) Maximum axial forces versus the loading rate.

frame structure in China. The column height is 3.72 m, corresponding to the net height of the ground floor. The column is fixed at the base, and a 50 mm end plate is added at the top to ensure uniform load distribution during axial force application. The initial axial force is designed to be 500 kN. To represent explosions caused by a passenger/cargo van, as outlined in FEMA 428 [11], a TNT equivalent mass of 1,814 kg is used as the explosive charge. Fig. 8 illustrates the explosion scenarios, where the damage levels of the steel columns are evaluated for various combinations of standoff distance (R = 6–10 m) and angle of incidence (α = 0°, 45° and 90°) under the passenger/cargo van explosion. Here, H = 1.37 m represents the height of burst. The angle of incidence α is defined as the angle between the line connecting the charge centre and the mid-span centre of the column and the strong axis of the column (Fig. 9).

Fig. 10 shows the numerical model of the steel column under scenario with R = 7 m and α = 45°. The FE model, including S-ALE, Lagrangian mesh sizes, material models, and numerical methods all employ the validated methods from Section 2 and will not be repeated

www.witpress.com, ISSN 1743-3509 (on-line)

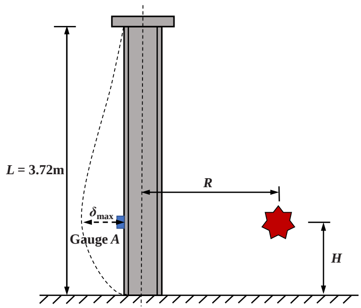

Figure 8: Diagram of explosion scenarios.

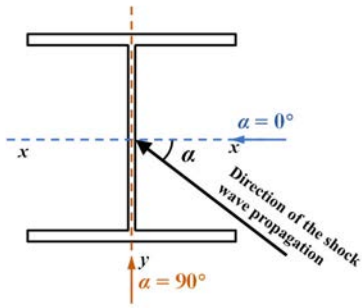

Figure 9: Definition of angle of incidence.

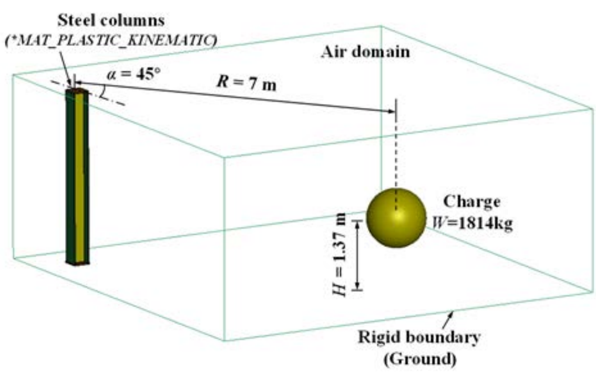

Figure 10: Numerical model of the scenario with R = 7 m, α = 45°.

here. It should be noted that this study ignores the influence of charge shape, i.e. all explosives are modelled as spherical charges. Regarding the boundary conditions, except for the rigid boundary representing the ground as shown in Fig. 10, the other five faces of the air domain are all set as non-reflecting boundaries. All translations and rotations are constrained for the nodes on the top face of the endplate and the bottom face of the column to realize a total fixed support ($\delta_x = \delta_y = \delta_z = 0$, $\theta_x = \theta_y = \theta_z = 0$).

3.2 Results and discussion

Using the numerical model mentioned above, the damage modes of the steel columns under different explosive scenarios will be discussed first in this section. Then the damage evaluation will be conducted based on residual capacity.

3.2.1 Damage modes

When the standoff distance is relatively small, i.e. R = 6 m, at an angle of incidence α = 0°, the shock wave primarily acts on the web, causing the column to bend about its weak axis. Additionally, multiple reflections of the shock wave within the flange–web–flange region result in the outward opening of the two half-flanges and backward deformation of the web along the shockwave propagation direction, accompanied by tearing at the flange–web connections (Fig. 11(a)). At α = 45°, when the shock wave reaches the steel column, it splits into two parts at the edge of the blast-facing flange: one part propagates along the flange, while the other enters the flange–web–flange region, leading to multiple reflections (Fig. 11(b)). Under such shock wave impacts, the steel column experiences tearing at the flange–web connections and shear failure at the base of the web. At α = 90°, the shock wave impinges the flange facing the charge, resulting in shear fractures in the web at two locations: near the base and slightly below the burst height. Additionally, significant backward bending of the two half-flanges and separation at the flange–web connection are observed.

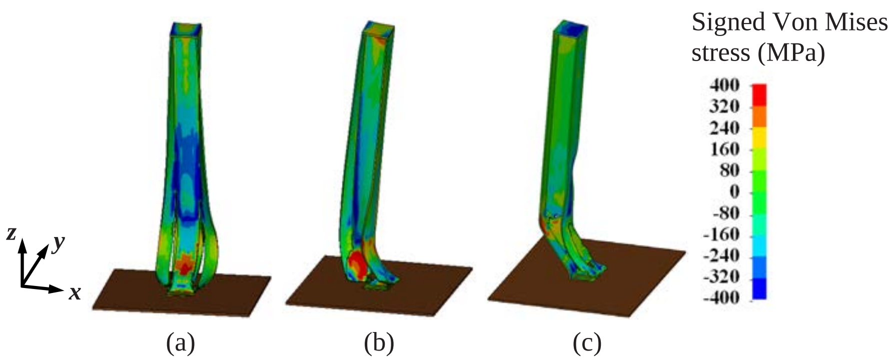

Figure 11: Damage modes of steel columns after the blast under R = 6 m. (a) α = 0°; (b) α = 45°; and (c) α = 90°.

At relatively large standoff distances, i.e. R = 7–10 m, the steel columns generally do not fracture after the blast. Instead, damage primarily manifests as a combination of overall bending, torsion, and local buckling. Fig. 12 illustrates the damage modes of the steel column at R = 8 m and α = 0°, 45° and 90°. At the scenario with α = 0°, the column primarily bends about its weak axis, with a significant hogging moment at the base leading to high stress concentrations. Additionally, substantial shear forces induced by the shockwave result in large stresses at the flange–web connections (Fig. 12(a)). At α = 45°, the column experiences biaxial bending, torsion, and local buckling. The web exhibits diagonal shear deformation along the dashed line at the column base indicated in Fig. 12(b). At α = 90°, the column primarily bends about its strong axis, with significant shear forces at the base primarily borne by the web (Fig. 12(c)).

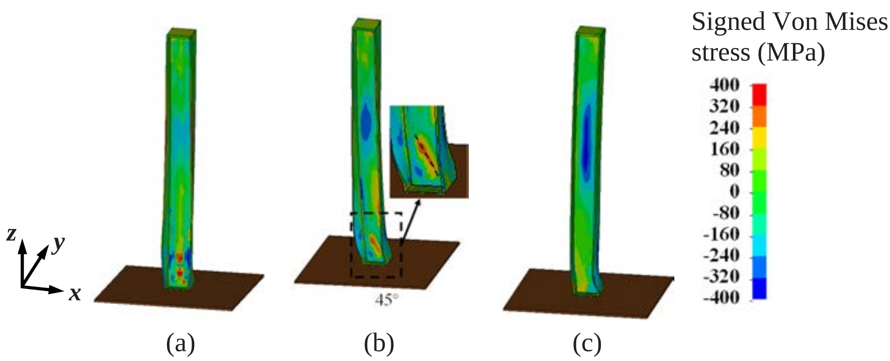

Figure 12: Damage modes of steel columns after the blast under R = 8 m: (a) α = 0°; (b) α = 45°; and (c) α = 90°

3.2.2 Damage assessment

After determining the damage modes of the steel columns, an axial load is applied to the top endplate using displacement control until the column fails completely. The resulting load-displacement curves for steel columns under various standoff distances and angles of incidence are shown in Fig. 13. The corresponding damage index (DI) for each scenario is presented in Fig. 14.

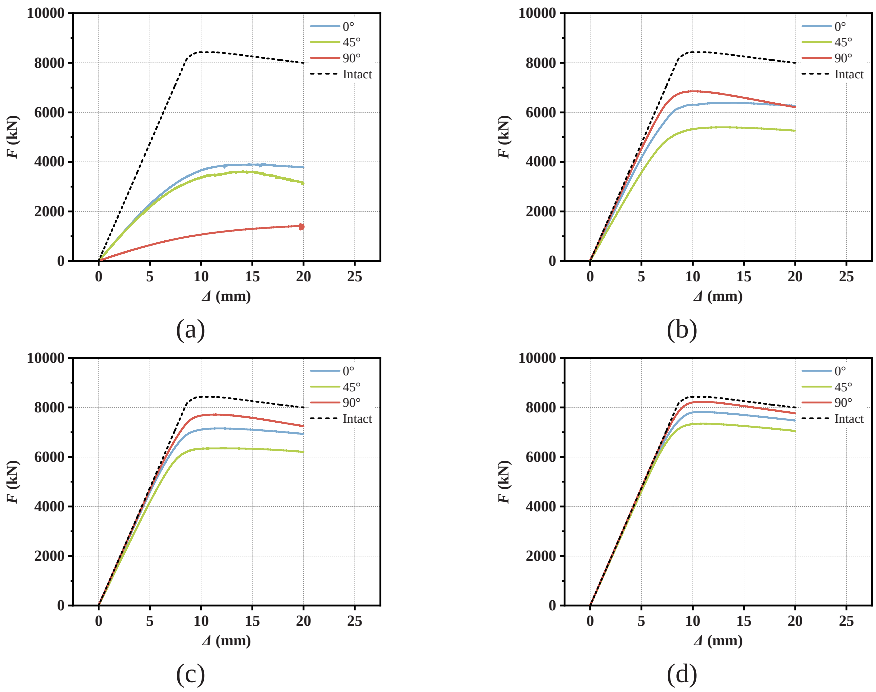

Figure 13: Force-displacement curves of the columns at: (a) R = 7 m; (b) R = 8 m; (c) R = 9 m; and (d) R = 10 m.

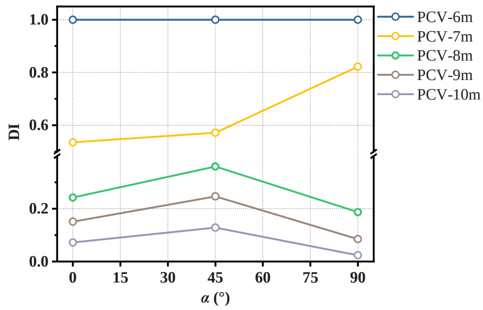

Figure 14: Damage index of the columns versus angles of incidence at diverse standoff distances.

At a standoff distance of R = 6 m for all angles of incidence, the steel columns lose their axial load-bearing capacity due to tearing and shear failure. For R = 7 m at α = 0° and 45°, the columns primarily experience bending or a combination of bending and torsion, which do not compromise the cross-sectional area or overall integrity, corresponding to DI values of 0.54 and 0.57. At α = 90°, the load-displacement curves show a significant reduction in capacity and stiffness, attributed to pronounced shear failure at the base, resulting in a weakened section composed only of the two flanges, corresponding to DI = 0.82. For R = 8–10 m, the load-displacement curves for all angles of incidence resemble those of undamaged columns, with no significant reduction in post-blast stiffness, corresponding to DI values of 0.02–0.25, indicating low levels of damage.

4 CONCLUSION

In this study, the damage modes and residual load-bearing capacity of a full-scale H-section steel column subjected to a vehicle explosion of passenger/ cargo van are investigated. The numerical models for the blast phase and residual capacity phase are validated using blast tests by Nassr et al. [8], [9] and axial compression tests by Zhao et al. [10], respectively. The standoff distance and angle of incidence are varied to observe the column's response and residual capacity under blast loading.

The results show that at smaller standoff distances, the shock wave primarily impacts the flange–web–flange region at α = 0°, causing tearing failure at the flange–web connections. At α = 90°, the shock wave mainly impacts the blast-facing flange, leading to shear fracture at the column base. At α = 45°, both tearing and shear fractures occur simultaneously.

At larger standoff distances, the column exhibits no significant fractures but experiences overall bending or torsion with local buckling. The post-blast damage modes can be used to evaluate damage levels. When significant tearing or shear fracture occurs, the damage index (DI) exceeds 0.8, indicating potential collapse and substantial stiffness loss. When only bending or torsion occurs without significant fractures, the stiffness remains relatively unchanged, with a slight reduction in load-bearing capacity, and the DI is less than 0.6.

ACKNOWLEDGEMENTS

The authors would like to thank the National Natural Science Foundation of China (grant number: 52278521) and the Fundamental Research Funds for the Central Universities for financial support to carry out this research.

REFERENCES

[1] Magallanes, J.M., Martinez, R. & Koenig J.W., *Experimental Results of the AISC Full-Scale Column Blast*, The American Institute of Steel Construction: USA, 2006.

[2] Morrill, K.B., Crawford, J.E., Magallanes, J.M. & Choi, H.J., Development of simplified tools to predict blast response of steel beam-column connections. *Structural Engineering Research Frontiers*, 2007.

[3] Grisaro, H.Y., Packer, J.A. & Seica, M.V., Experimental and numerical investigation of bare and strengthened wide-flange sections subject to near-field blast loading. *Journal of Structural Engineering*, **147**(9), 04021139, 2021.

[4] Grisaro, H.Y., Seica, M.V., Packer, J.A. & Li, W., Strong-axis response of steel I-sections subjected to close-in detonations. *International Journal of Protective Structures*, **12**(3), pp. 347–376, 2021.

[5] Grisaro, H.Y., Packer, J.A. & Seica, M.V., Weak axis response of steel I-sections subjected to close-in detonations. *Journal of Constructional Steel Research*, **160**, pp. 189–206, 2019.

[6] Remennikov, A.M. & Uy, B., Explosive testing and modelling of square tubular steel columns for near-field detonations. *Journal of Constructional Steel Research*, **101**, pp. 290–303, 2014.

[7] Gangolu, J. & Grisaro, H.Y., Axial load ratio effect on wide-flange columns subjected to far field detonations. *Journal of Constructional Steel Research*, **223**, 109009, 2024.

[8] Nassr, A.A., Razaqpur, A.G., Tait, M.J. & Foo, S., Experimental performance of steel beams under blast loading. *Journal of Performance of Constructed Facilities*, **26**(5), pp. 600–619, 2012.

[9] Nassr, A.A., Razaqpur, A.G. Tait, M.J., Campidelli, M. & Foo, S., Strength and stability of steel beam columns under blast load. *International Journal of Impact Engineering*, **55**, pp. 34–48, 2013.

[10] Zhao, H., Wang, R., Li, Q.M., Wu, H., Hou, C.C. & An, G.Q., Experimental and numerical investigation on impact and post-impact behaviours of H-shaped steel members. *Engineering Structures*, **216**, 110750, 2020.

[11] Department of Homeland Security, *Primer to Design Safe School Projects in Case of Terrorist Attacks and School Shootings (Edition 2)*, Federal Emergency Management Agency: USA, 2012.